Asian Journal of Chemistry; Vol. 28, No. 6 (2016), 1297-1303

ASIAN JOURNAL OF CHEMISTRY

http://dx.doi.org/10.14233/ajchem.2016.19660

Synthesis of Graphene Titanium Dioxide Composites as Photocatalytic Materials for Degradation of Moderacid Black

THANH XUAN NGUYEN[1], MO THI NGUYEN[1], HUNG VAN NGUYEN[2] and HUNG VAN HOANG[1,*]

[1]Faculty of Chemistry, Hanoi National University of Education, 136 Xuan Thuy Cau Giay, Hanoi, Vietnam
[2]Faculty of Physics, Hanoi National University of Education, 136 Xuan Thuy Cau Giay, Hanoi, Vietnam

*Corresponding author: Tel: +84 4 38330842; E-mail: hunghv@hnue.edu.vn; hvhungsp@yahoo.com

Received: 8 October 2015; *Accepted*: 15 January 2016; *Published online*: 29 February 2016; AJC-17795

Graphene titanium dioxide composites with different ratios of graphene to TiO_2 have been successfully synthesized by a facile hydrothermal method using graphite and titanium tetrachloride as precursors. The composites were characterized by scanning electron microscope, Raman and ultraviolet-visible spectroscopies, X-ray diffraction and thermogravimetric analysis. A composite with titanium content of 20 % was revealed to be the most thermally stable in comparison to other composites, with the most uniform distribution of TiO_2 on graphene sheets. The photodegradation study and thermogravimetric analysis showed that the composite with 20 % of titanium is a very stable material. After 15 times use, the photodegradation efficiency remained almost constant with the value of 99.38 %.

Keywords: Graphene, TiO_2, Hydrothermal method, Photocatalyst, Moderacid black.

INTRODUCTION

The photocatalytic degradation of organic pollutants based on wide band gap semiconductors has attracted increasing attention during the past decades due to their capability of simultaneous harvesting solar energy and driving chemical reactions *via* photo-excited charge carriers and activated electronic states [1]. Among various semiconductor materials studied, TiO_2 has been recognized as the most common candidate for widespread environmental applications because of its long-term stability, non-toxicity, controllable structure and morphology and low price [2,3]. However, there are three bottlenecks to hinder its practical applications. One is that the band gap of TiO_2 is 3.2 eV, hence it can absorb only the ultraviolet light (radiation with wavelength, $\lambda < 400$ nm), which accounts for about 4 % of the sunlight. The second drawback comes from the low separation probability of photo-induced electron-hole pairs in photocatalysts leading to the recombination of electron-hole pairs and therefore reducing the photocatalytic efficiency. The last one is due to the difficulty in collecting it for reusing because TiO_2 in the form of nano-particles can be dispersed in aqueous solution and, therefore, swept away after use. Up to now, various processes have been proposed *via* either doping or compound modification to narrow its band gap and enhance the photocatalytic activity in the range of the visible wavelength radiation [1,2,4,5]. However, further study is needed to produce materials which can offer the better requirements.

Graphene, a flat one-atom-thick monolayer consisting of carbon atoms tightly packed into a two dimensional (2D) honeycomb sp^2 carbon lattice, is another allotrope of carbon beside fullerenes and carbon nanotube. It has been intensively considered due to the unique physical, chemical and mechanical properties. It processes high conductivity at room temperature [6], high specific surface area up to 2630 $m^2 g^{-1}$, complex band structure with conduction and valence bands overlapping for a multi-layer graphene, *etc*. [7]. Among the applications of graphene, integrating graphene with other inorganic materials to fabricate composites or hybrids is the focus. Particularly, the composite of TiO_2 and graphene has been considered as a potential photocatalyst in the treatment of polluted air and water [8,9]. It is believed that, a combination of graphene and TiO_2 forming composite can reinforce photocatalytic efficiency in which graphene acts as an excellent conductor to spread generated electron-hole pairs on TiO_2 due to the interaction of TiO_2 and graphene and therefore hinder the recombination of these electron-hole pairs raising the photocatalytic efficiency [10]. Graphene-TiO_2 composites have been successfully fabricated by various ways in recent years. Liang *et al.* [11] reported that graphene-TiO_2 nanocrystal hybrid has been prepared by directly growing TiO_2 nanocrystals on graphene oxide sheets. The direct growth of the nanocrystals on graphene oxide sheets was achieved by a two-step method, in which TiO_2 was first coated on graphene oxide sheets by hydrolysis and crystallized into anatase nanocrystals by hydrothermal

treatment in the second step. Kamat *et al*. [12] reported that graphene-TiO_2 composite is obtained *via* UV illuminated suspension of GO-TiO_2 under inert atmosphere condition, inhibiting the UV light as reducer [12]. Liu *et al*. prepared the self-assembly of TiO_2 with graphene composites in the stabilization of graphene in aqueous solution by assistance of anionic sulfate surfactant [13].

In this paper, we report a facile hydrothermal process for preparation of graphene-TiO_2 composites with different ratios of graphene to titanium(IV) oxide using graphite and titanium(IV) chloride as precursors. The characterization and photocatalytic activity of the obtained materials assessed by degradation of Moderacid Black aqueous solution under UV-visible radiation are also reported.

EXPERIMENTAL

Titanium(IV) chloride was purchased from Merck and used as received. The graphite (GR) flake was purchased from Sigma Aldrich. Distilled water was used, Moderacid Black (MDB) and all other chemicals were analytical grade reagents and used as received.

Preparation of graphene oxide (GO): Graphene oxide was synthesized from graphite powder by a modified Hummer's method [14]. In a 1000 mL beaker, 4 g of graphite and 2 g of $NaNO_3$ were mixed with 100 mL of concentrated H_2SO_4 (98 %). The mixture was stirred for 3 h at ambient temperature. During stirring, 5 g of $KMnO_4$ was slowly added to the suspension and the temperature was maintained at ambient temperature. After addition of $KMnO_4$, the reaction mixture was then stirred at 30 °C for 7 h. Then, 250 mL of dilute H_2SO_4 (5 %) was slowly added to the mixture with vigorous stirring. The diluted suspension was again stirred at 90 °C for 4 h. Finally, 50 mL of 30 % H_2O_2 was added. The whole reaction mixture was washed by centrifuging with 5 % H_2SO_4 followed by distilled water for 6 to 8 times and filtered to obtain gray graphene oxide sheets.

Hydrothermal preparation of graphene TiO_2: Suspension of graphene oxide was prepared by mixing graphene oxide with water under vigorous stirring. Then the $TiCl_4$ in ethanol solution was slowly added to graphene oxide suspension followed by stirring for another 1 h. The mixture was finally transferred to 200 mL autoclave maintained at 200 °C for 24 h. The resulting composite was obtained by filtering the precipitated portion following by washing with distilled water and drying at 100 °C for 12 h. The amount of $TiCl_4$ solution added to graphene oxide suspension varied in order to produce composite samples with different GO/TiO_2 weight ratios with the TiO_2 percentage of 5, 10, 20, 40, 60 and 80 wt %. For convenience, composite samples are denoted as G$XTiO_2$ (X is percentage of TiO_2 in samples corresponding to the values of 5, 10, 20, 40, 60 and 80). Pure TiO_2 was prepared similarly to above procedure. The $TiCl_4$ in ethanol solution was added slowly to distilled water under vigorous stirring and then transferred to 200 mL autoclave maintained at 200 °C for 24 h. The obtained precipitate was filtered, washed and dried at 100 °C for 12 h.

Characterization: Scanning electron microscopy (SEM) was performed by a Hitachi S-4800 field emission scanning electron microscope at 5 kV. X-ray diffraction (XRD) patterns of the samples were recorded on a Bruker-D5005 powder X-ray diffractometer using copper K_α-radiation with λ = 1.5406 Å. Raman spectroscopy was conducted using LAB RAM HR800, HORIBA-France. UV-visible absorption spectra were recorded by Jasco V670 spectrophotometer. Thermogravimetric analysis (TGA) was carried out on a Shimazu DTG-60H instrument at a heating rate of 10 °/min under air flow.

Photocatalytic activity: The photocatalytic activity of the photocatalyst was confirmed by the degradation of a common dye Moderacid black used in textile industry, under radiation of sun light. Photocatalyst (2.5 mg) was dispersed into 20 mL of Moderacid black solution with the concentration of 40 mg/L and then the mixture was stirred for several seconds, after that the mixture was exposed to radiation of sun light (the temperature is about 33 °C). The samples were analyzed every 60 min using UV-visible spectrophotometer. Experiments were carried out under sun light irradiation during the time from 10 am to 4 pm of the shiny day without cloud and with the temperature of around 34 °C.

RESULTS AND DISCUSSION

X-ray diffraction: Fig. 1 shows the XRD patterns of graphite powder, graphene oxide, graphene and G$XTiO_2$ composites with different contents of TiO_2 ranging from 5 to 80 %.

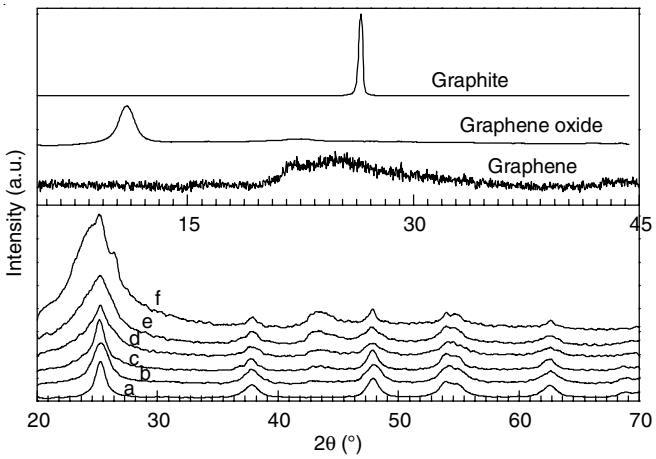

Fig. 1. X-ray diffraction patterns of G$XTiO_2$ composites: (a) G80TiO_2, (b) G60TiO_2, (c) G40TiO_2, (d) G20TiO_2, (e) G10TiO_2 and (f) G5TiO_2 composites

The XRD pattern of pure pristine graphite exhibits a sharp peak at about 2θ = 26.5° correlating to an interlayer space of 3.36 Å. While, reflection angle of graphene oxide shifts to the lower value of about 11° correlated to interlayer distance of 8.80 Å. The increase in *d*-space of graphene oxide suggests that functional groups were formed after oxidation of graphite. For graphene, in XRD pattern appears a broad reflection slightly shifted to lower value in comparison with reflection angle of graphite. This relative small shift reveals the presence of oxygen functional groups in graphene leading to slightly higher value of *d*-spacing compared with the case of graphene oxide [15].

All XRD patterns of G$XTiO_2$ composites exhibit diffraction peaks at 2θ = 25.3, 37.0, 48.0, 54.0, 55.0 and 62.7° which are all characteristic peaks of TiO_2 anatase phase [16]. It was

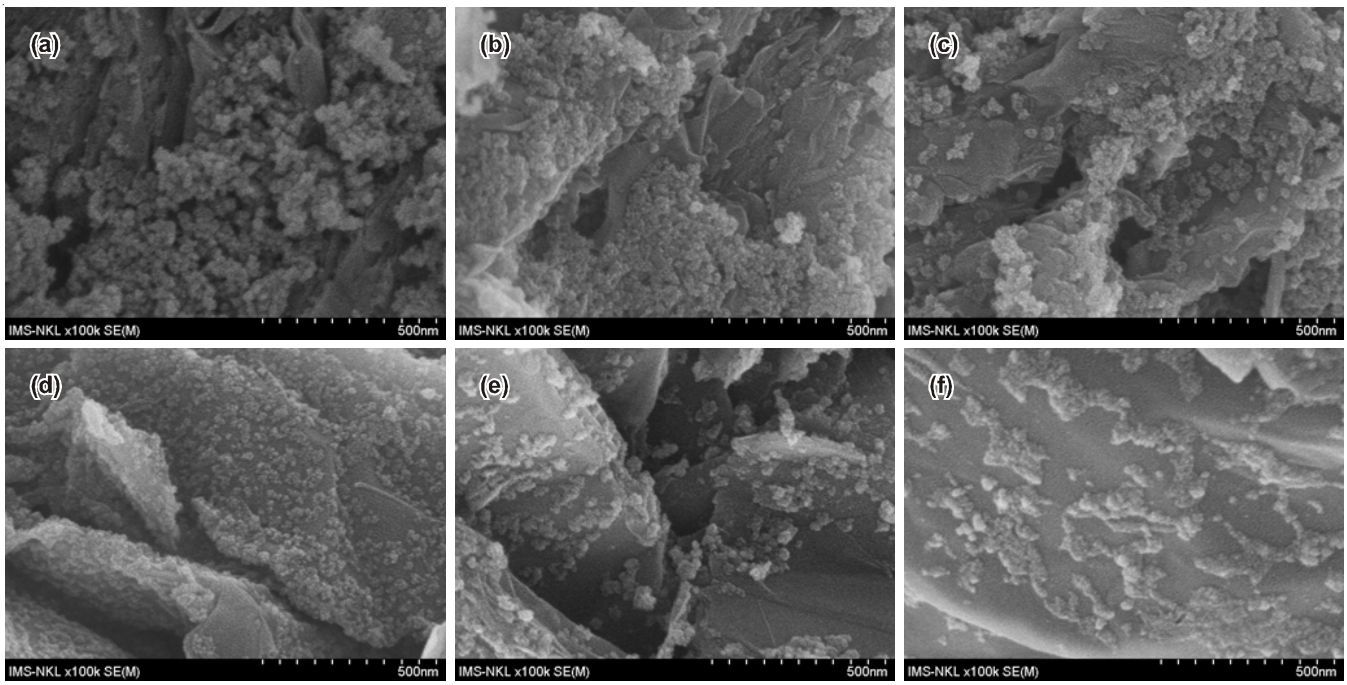

Fig. 2. SEM images of $GXTiO_2$ composites: (a) $G80TiO_2$, (b) $G60TiO_2$, (c) $G49TiO_2$, (d) $G20TiO_2$, (e) $G10TiO_2$, (f) $G5TiO_2$ composites

agreed that rutile form of TiO_2 can only be formed under highly acidic conditions therefore, in our case rutile form was hardly formed [17]. Peaks in patterns are all relatively broad. This result suggests that the TiO_2 particles formed on the graphene sheets with small particle size. In comparison to two other forms of TiO_2 (rutile and brookite), anatase form has higher forbidden bandwidth and larger specific surface area which would be beneficial to the photocatalytic processes. The XRD patterns of the $GXTiO_2$ composites are similar to the XRD pattern of pure TiO_2 reported in [18], illustrating that the existence of graphene did not influence the particles of pure TiO_2 fabricated on it [19,20].

Morphology analysis: In order to get more information of materials, the prepared $GXTiO_2$ composites were characterized using scanning electronic microscope. The results are shown in Fig. 2. From images, one can see that TiO_2 particles are spread on surface of graphene sheets. There is a difference in distribution of TiO_2 at different samples where contents of graphene in samples are varied. The particle density of TiO_2 on the surface of graphene sheets increases as TiO_2 content in sample increases. The most uniform distribution can be seen in Fig. 2d in the sample with 20 wt % of TiO_2. In samples with more or less than 20 wt % of TiO_2, the accumulation of TiO_2 particles and non-uniform distribution of TiO_2 particles on graphene sheets can be observed.

Thermogravimetric analysis (TGA): The composition and structure of the $GXTiO_2$ composites were further studied by thermogravimetric analysis. TGA curves (Fig. 3) of graphite and graphene oxide, graphene and $GXTiO_2$ composites were obtained in air atmosphere. As expected, graphite is highly stable up to 700 °C, while most of mass of graphene oxide is lost rapidly at the temperature of under 200 °C. This can be explained due to pyrolysis of labile oxygen-containing functional groups yielding a vigorous release of steam, CO and CO_2 gases and therefore leading to the large mass loss [21,22].

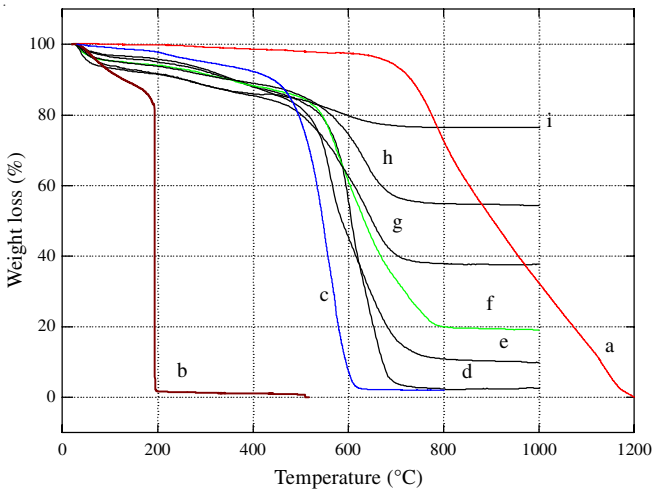

Fig. 3. Thermogravimetric analysis of: (a) graphite, (b) graphene oxide, (c) graphene, (d) $G5TiO_2$, (e) $G10TiO_2$, (f) $G20TiO_2$, (g) $G40TiO_2$, (h) $G60TiO_2$ and (i) $G80TiO_2$ composites

In contrast with graphene oxide, TGA curve of graphene shows the significantly improved thermal stability indicating the removal of oxygen-containing functional groups in graphene oxide sheets in the reduction step [22].

As shown in Fig. 3, TGA curves of all the composites reveals the improvement in thermal stability of composites in comparison to graphene and graphene oxide. At the temperature under 200 °C, only small amount of composites is lost (5.0; 4.0; 6.0; 8.5, 6.0 and 8.0 % for $G5TiO_2$, $G10TiO_2$, $G20TiO_2$, $G40TiO_2$, $G60TiO_2$, $G80TiO_2$, respectively). This mass loss is due to the de-intercalation of H_2O from graphene [23]. At the temperature ranging from 550 to 700 °C, the oxidation of graphene in composites occurs vigorously and therefore, most of the graphene in composites is lost in this range of temperature. In comparison to graphene and graphene oxide, all composites have higher value of major degradation-

temperature as can be seen in Fig. 3 and Table-1. This can be explained due to the interaction between TiO_2 and oxygen in residual functionalities on graphene sheets [24].

TABLE-1
TGA DATA OF GXTiO_2 COMPOSITES

Sample	Weight loss (%) at temperature (°C)			Major degradation temperature (°C)	Weight retention (%) at 700 °C
	200	400	500		
Graphite	0.20	0.88	2.08	777	95.63
GO	98.29	98.92	99.24	194	0
Graphene	2.18	7.64	21.53	544	2.15
G5TiO_2	5.00	12.00	17.50	600	4.00
G10TiO_2	4.00	12.00	18.00	558	84.00
G20TiO_2	6.00	12.00	15.00	560	66.50
G40TiO_2	8.50	14.50	20.00	636	50.50
G60TiO_2	6.00	11.00	14.50	562	54.50
G80TiO_2	8.00	14.00	15.50	600	76.50

It is interesting that, weight loss of graphene in sample G20TiO_2, in the range from 550 to 700 °C, takes place slower than that of in other GXTiO_2 samples with less steeper slope (Fig. 3f). The mass reduction of sample lasts until 790 °C, while weight loss of other GXTiO_2 samples maintains less than 750 °C. As mentioned above, the interaction of oxygen atom of functional group on graphene sheets and TiO_2 can increase the thermal stability of composites. However, for G20TiO_2, the better distribution of TiO_2 on graphene sheets (Fig. 2d), in comparison to other composites, may also improve its thermal stability.

Raman spectroscopy: In order to prove the formation of graphene from reduction of graphene oxide and interaction between TiO_2 and oxygenated functional groups, graphene oxide, graphene and G20TiO_2 composite were further characterized by Raman spectroscopy. The obtained spectra were shown in Fig. 4. As can be seen from the spectra, two intensity peaks at 1327 and 1600 cm^{-1} are dominated in spectrum of graphene oxide. These peaks are referred to D and G bands, respectively. Similarly to spectrum of graphene oxide, spectrum of graphene also consists of D and G bands. However, the D/G intensity ratio (I_D/I_G = 1.48) is much higher than that of graphene oxide (I_D/I_G = 0.87), which indicates a decrease in the average size of sp^2 domains upon reduction of graphene oxide to form graphene and an increase in edge planes as well as the degree of disorder in the synthesized graphene sheets [25]. For G20TiO_2, in the spectrum, peaks appear at (150, 398, 635, 1327 and 1595 cm^{-1}) in the range from 140 to 1650 cm^{-1} charac-teristic for both graphene and anatase form of TiO_2 in the composite [26]. Compare with spectrum graphene, the peak assigned to G band G20TiO_2 slightly shifts to higher wavenumber. This shift, one more time, confirms the strong interaction between TiO_2 and oxygenated functional group on graphene sheets [27].

UV-visible spectroscopy: UV-visible spectra of graphene, graphene oxide and G20TiO_2 composite are shown in Fig. 5. Values of band-gap for pure TiO_2 and TiO_2 in composite were estimated to be 3.76 and 3.49 eV, respectively. The pure TiO_2 mainly absorbs in the region of UV radiation, while graphene and G20TiO_2 absorb both UV and visible regions. The absorbance

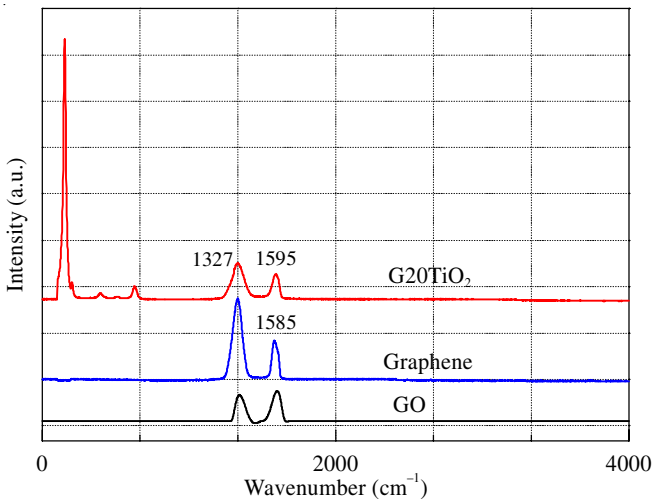

Fig. 4. Raman Spectra of graphene oxide, graphene and G20TiO_2 composite

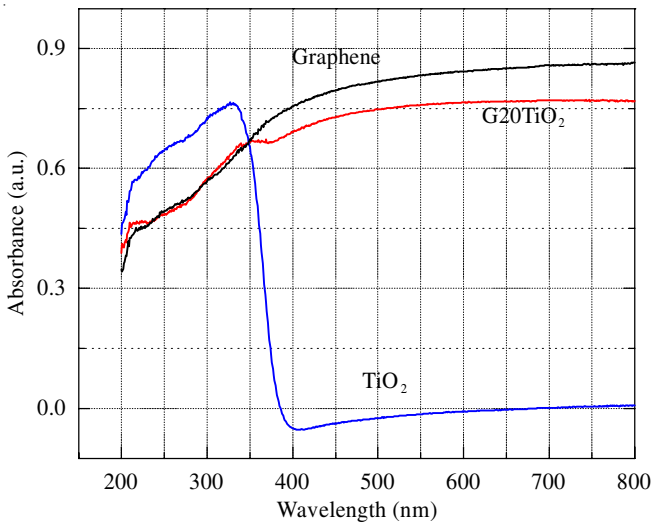

Fig. 5. UV-visible spectra of graphene oxide, graphene and G20TiO_2 composite

of composite in UV region is smaller than that of TiO_2 and in visible region is less than that of graphene. These decreases may be explained due to the lower concentration of TiO_2 in composite compared with pure TiO_2 and the lower concentration of graphene in composite compared with graphene itself. As can be seen in Fig. 5, it is interesting to note that the absorbance band at 330 nm in spectrum of pure TiO_2 slightly shifts to 356 nm in spectrum of G20TiO_2. This small shift may be due to the interaction of TiO_2 with oxygen of residual functional groups on graphene sheets.

Photoatalytic reactivity: In order to study the phototcatalytic activity of GXTiO_2 composites, a number of experiments were carried out over GXTiO_2, in which several factors affecting phototcatalytic activity were tested using Moderacid black (MDB), a common dye used in textile industry.

Effect of TiO_2 content: Experiments were carried out as follows: 2.5 mg of each GXTiO_2 material was mixed thoroughly in dark with 20 mL of 40 mg/L Moderacid Black solution. pH of the solution was established by itself with value of 6.5. The mixture was then transferred to 50 mL Erlenmeyer flask with stopper and exposed to the sun light irradiation for 5 h. The obtained results are shown in Fig. 6.

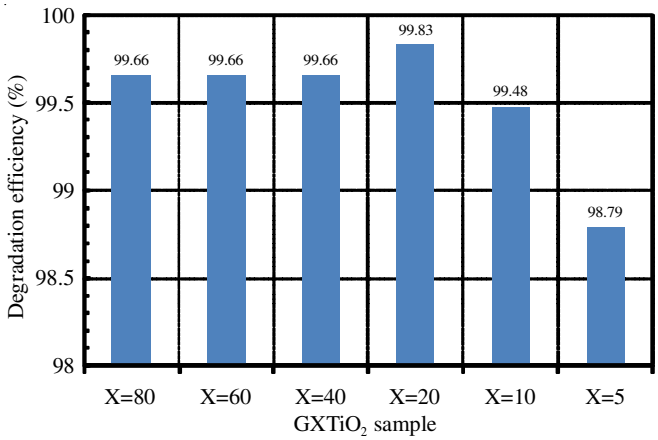

Fig. 6. Photodegradation efficiency of $GXTiO_2$ after 5 h exposure to sunlight irradiation

As can be seen in Fig. 6, $G20TiO_2$ reaches the highest degradation efficiency of 99.83 % and $G5TiO_2$ gets the lowest efficiency of 98.79 %. The highest efficiency of $G20TiO_2$ in comparison to other $G20TiO_2$ composites can be explained due to the most uniform distribution of TiO_2 on graphene in $G20TiO_2$ sample. The better uniform distribution of TiO_2 would prevent better the re-combination of photo-generated electrons and holes, therefore increases the degradation efficiency. For this reason, $G20TiO_2$ will be chosen for all experiments.

Effect of composite mass: In order to optimize the mass of photocatalyst used in photocatalytic reaction, a series of similar experiments was carried out in which only mass of $G20TiO_2$ was varied in the range of 1.0, 2.5, 5, 7.5, 10.0 and 12.5 mg. The experiments were carried out as previous experiments with exposure time of 5 h. The experimental results are shown in Fig. 7.

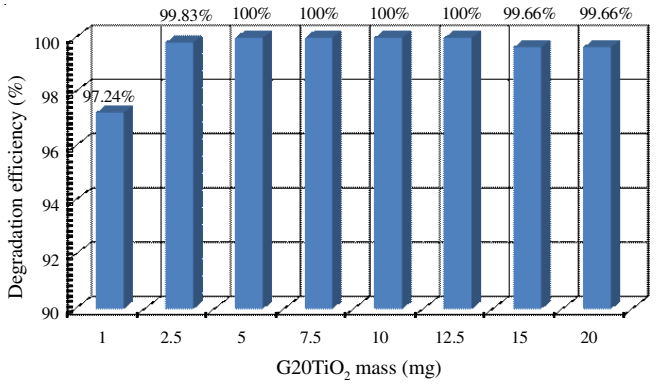

Fig. 7. Dependence of efficiency on the mass of $G20TiO_2$ composite

The degradation efficiency increases as the mass of photocatalyst increases and reaches 99.83 and 100 % corresponding with 2.5 and 5.0 mg of composite, respectively. The degradation efficiency can reach 99.83 %, almost equal to 100 %, though composite mass used is half of that in the case getting maximum degradation efficiency (100 %). With economic aspect, all following experiments will be carried out with 2.5 mg of $G20TiO_2$.

Effect of exposure time, pH and concentration of dye: Effects of exposure time, pH and concentration of dye solution on degradation efficiency were investigated in order to choose the best conditions for photo-degradation reaction of Moderacid black. Experiments were carried out at different pH values, illumination time and concentrations of Moderacid black solution. All experiments were done under 5 h illuminating by sunlight for exposure-time test experiments, 4 h for dye concentration and pH tests. Order of experiments was done as follows: exposure time, dye concentration and the obtained results are depicted on Table-2.

TABLE-2
EFFECTS OF EXPOSURE TIME (t), CONCENTRATION OF DYE (C) AND pH OF SOLUTION ON DEGRADATION EFFICIENCY (E)

t (min)	E (%)	C (mg L^{-1})	E (%)	pH	E (%)
60	87.76	10	100	5.0	99.83
90	91.55	15	100	5.5	99.83
120	95.69	20	99.83	6.0	99.83
150	96.90	25	99.86	6.5	99.83
180	97.93	30	99.89	7.0	99.83
210	99.14	35	99.90	7.5	99.83
240	99.83	40	99.83	8.0	99.83
300	99.83	50	99.86	8.5	99.83
–	–	60	99.89	9.0	98.61
–	–	70	99.85	9.5	98.27
–	–	80	99.87	10	98.43
–	–	90	99.89	–	–
–	–	100	99.86	–	–
–	–	110	95.11	–	–
–	–	120	87.76	–	–

As result shown in Table-2, the optimized exposure time for degradation reaction of 40 mg/L Moderacid black solution is 240 min with the degradation efficiency of 99.83 %. However, when concentration of Moderacid black varied, the best concentration which could be used for the degradation reaction is 100 mg/L with the reaction efficiency almost equal to that with concentration. At concentration greater than 100 mg/L, the efficiency is slightly reduced. This may be explained as follows: at high Moderacid black concentration, the solution will shield radiations which may reach to composite leading to the less generated electron-hole pairs and low degradation efficiency.

According to the data on Table-2, pH values ranging from 5 to 10 do not change much the photocatalytic activity of the composite. Moderacid black is a dye used commonly in textile industry. Moderacid black solution has pH of around 6.5 by its nature. The surface of TiO_2 is amphoteric with the pH_{pzc} (point of zero charge) of around 6.3. At high pH value, Moderacid black, TiO_2 surface and graphene sheet with residual oxygenated functionalities become negative charge. Therefore, repulsion forces between these negative species are created [28,29]. These forces may affect the photocatalytic reaction and reduce the efficiency of reaction.

Recyclability of $G20TiO_2$: The recyclability of $G20TiO_2$ in photodegradation reaction of Moderacid black was tested as following procedures: the mixture of 2.5 mg of $G20TiO_2$ and 20 mL of 40 mg/L Moderacid black solution was exposed to sunlight irradiation for 4 h. The mixture was then decanted to separate the liquid portion. The remain composite was reused by adding 20 mL of 40 mg/L Moderacid black solution in and exposed to the sun light irradiation for 4 h. These steps were repeated 14 times more. After the final experiment, the compo-

site was separated and analyzed by thermogravimetric analysis. The results are shown in Fig. 8.

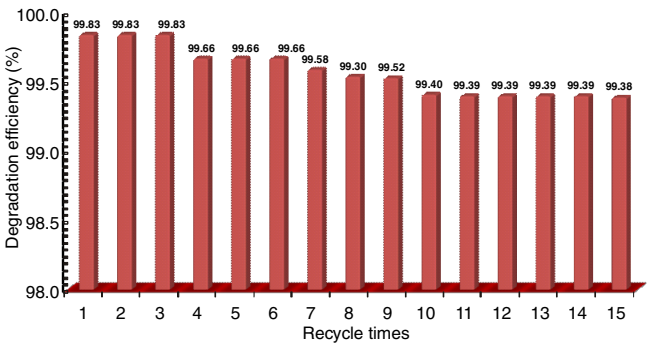

Fig. 8. Recyclability of G20TiO_2 composite

As shown in Fig. 8, the photocatalytic efficiency of G20TiO_2 remains almost constant after 15 times use. After the first three times use, the efficiency drops slightly from 99.83 to 99.66 % and keeps constant for the next three uses. From the 7th to 11th use, the efficiency reduces continuously with a small amount. These small changes can be explained due to the lost of composite during decanting processes, in which a very small amount of composite dispersed in solution is swept way. These results suggest that the prepared G20TiO_2 composite is very stable composite in both chemical and photocatalytic aspects. The stability of composite may be due to the good chemical interaction between TiO_2 and oxygenated functional group as mentioned in Raman and UV-visible spectroscopy.

Thermogravimetric analysis was carried out for G20TiO_2 after 15 times use to check the stability of composite for reusable application. TGA curves of composite before and after photodegradation reaction in Fig. 9 show the similar trend. The mass loss starts occurring slowly when the temperature starts increasing, as the result of evaporation of water adsorbed on composite surface and the combustion of functional groups on graphene sheets. The major mass loss occurs in the range from 500 to 790 °C with respect to the combustion of carbon atoms in graphene sheets. The most important information from TGA curves is that both composites before and after photodegradation reaction have similar composition of about 20 wt % of TiO_2 (TGA curves in Fig. 9). This information proves

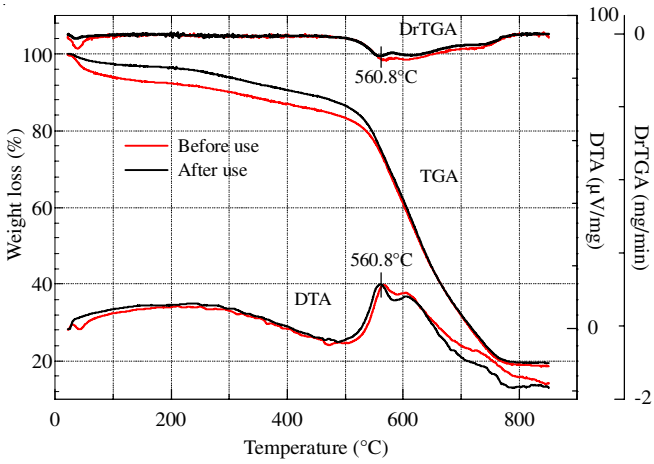

Fig. 9. Recyclability of G20TiO_2 composite

the good stability of G20TiO_2 composite in photodegradation reaction as a result of interaction between TiO_2 and oxygenated functionalities on graphene sheets. This interaction may enhance photodegradation efficiency of composite due to the scattering photogenerated electron-hole pairs on graphene sheets. In order to prove the enhancement of photodegradation efficiency of composite, the similar experiment was carried out using pure TiO_2 as photocatalyst. The obtained results show that in the case of TiO_2, the value of photodegradation efficiency was just 16.97 %, lower than that of G20TiO_2 composite (99.83 %).

Conclusion

In this work, we have prepared and characterized graphene titanium dioxide composites from graphite and titanium tetrachloride as precursors using a facile hydrothermal reaction. In all prepared composites, titanium dioxide exists in composites with characteristic peaks in XRD patterns of anatase form. The results obtained form the study show that composite composed of 20% of graphene possesses the most uniform distribution of TiO_2 on graphene sheets and thermal stability in comparison to other composites. In addition, it has the highest value of photodegradation efficiency, which remains almost constant after 15 time use. Furthermore, G20TiO_2 is very stable and its composition does not change after 14 recycle times. The high values of photodegradation efficiency, stability and recyclability which G20TiO_2 composite possesses may be explained due to the interaction of TiO_2 and oxygen atom of residual functional groups on graphene sheets. These properties make G20TiO_2 become a good candidate for treatment of waste water containing organic compounds.

ACKNOWLEDGEMENTS

The authors acknowledge the support from the Hanoi National University of Education through project: SPHN13-361TĐ.

REFERENCES

1. M.R. Hoffmann, S.T. Martin, W. Choi and D.W. Bahnemann, *Chem. Rev.*, **95**, 69 (1995).
2. U.M. Shahed, A.S. Mofareh and B.I. William, *Science*, **297**, 2243 (2002).
3. Y. Jing, L. Li, Q. Zhang, P. Lu, P. Liu and X. Lü, *J. Hazard. Mater.*, **189**, 40 (2011).
4. Y. Zhang, L. Fei, X. Jiang, C. Pan and Y. Wang, *J. Am. Ceram. Soc.*, **94**, 4157 (2011).
5. Z. Zhang, C. Shao, X. Li, C. Wang, M. Zhang and Y. Liu, *Appl. Mater. Inerfaces*, **2**, 2915 (2010).
6. A.K. Geim and K.S. Novoselov, *Nat. Mater.*, **6**, 183 (2007).
7. S. Park and R.S. Ruoff, *J. Nature Nanotech.*, **4**, 217 (2009).
8. H. Zhang, X. Lv, Y. Li, Y. Wang and J. Li, *ACS Nano*, **4**, 380 (2010).
9. X.Y. Zhang, H.P. Li, X.L. Cui and Y. Lin, *J. Mater. Chem.*, **20**, 2801 (2010).
10. X. Liu, L. Pan, T. Lv and Z. Sun, *J. Colloid Interf. Sci.*, **394**, 441 (2013).
11. Y.Y. Liang, H.L. Wang, H.S. Casalongue, Z. Chen and H. Dai, *Nano Res.*, **3**, 701 (2010).
12. G. Williams, B. Seger and P.V. Kamat, *ACS Nano*, **2**, 1487 (2008).
13. D.H. Wang, D.W. Choi, J. Li, Z.G. Yang, Z.M. Nie, R. Kou, D.H. Hu, C.M. Wang, L.V. Saraf, J.G. Zhang, I.A. Aksay and J. Liu, *ACS Nano*, **3**, 907 (2009).
14. X. Lu, H. Dou, S. Yang, L. Hao, L. Zhang, L. Shen, F. Zhang and X. Zhang, *Electrochim. Acta*, **56**, 9224 (2011).
15 A.V. Murugan, T. Muraliganth and A. Manthiram, *Chem. Mater.*, **21**, 5004 (2009).
16. H. Zhao, F. Su, X. Fan, H. Yu, D. Wu and X. Quan, *Chin. J. Catal.*, **33**, 777 (2012).

17. Y. Zhang, L. Wu, Q. Zeng and J. Zhi, *J. Phys. Chem. C*, **112**, 16457 (2008).
18. K. Thamaphat, P. Limsuwan and B. Ngotawornchai, *Kasetsart J. (Nat. Sci.)*, **42**, 357 (2008).
19. D. Wang, X. Li, J. Chen and X. Tao, *Chem. Eng. J.*, **198-199**, 547 (2012).
20. H. Zhao, F. Su, X. Fan, H. Yu, D. Wu and X. Quan, *Chin. J. Catal.*, **33**, 777 (2012).
21. S. Stankovich, D.A. Dikin, R.D. Piner, K.A. Kohlhaas, A. Kleinhammes, Y. Jia, Y. Wu, S.B.T. Nguyen and R.S. Ruoff, *Carbon*, **45**, 1558 (2007).
22. M. Shi, J. Shen, H. Ma, Z. Li, X. Lu, N. Li and M. Ye, *Colloids Surf. A*, **405**, 30 (2012).
23. K. Zhang, L.L. Zhang, X.S. Zhao and J. Wu, *J. Chem. Mater.*, **22**, 1392 (2010).
24. L.M. Pastrana-Martínez, S. Morales-Torres, V. Likodimos, J.L. Figueiredo, J.L. Faria, P. Falaras and A.M.T. Silva, *Appl. Catal. B*, **123-124**, 241 (2012).
25. X. Liu, L. Pan, Q. Zhao, T. Lv, G. Zhu, T. Chen, T. Lu, Z. Sun and C. Sun, *Chem. Eng. J.*, **183**, 238 (2012).
26. Y. Zhang, J. Xu, Z. Sun, C. Li and C. Pan, *Prog. Nat. Sci. Mater. Inter.*, **21**, 467 (2011).
27. H. Gao, W. Chen, J. Yuan, Z. Jiang, G. Hu, W. Shangguan, Y. Sun and J. Su, *Int. J. Hydrogen Energy*, **38**, 13110 (2013).
28. A. Piscopo, D. Robert and J.V. Weber, *Appl. Catal. B*, **35**, 117 (2011).
29. W.S. Hummers Jr. and R.E. Offeman, *J. Am. Chem. Soc.*, **80**, 1339 (1958).